Study of structural, magnetic and electrical properties on Ho-substituted BiFeO3

T. Durga Rao[a], T. Karthik[a, b], Adiraj Srinivas[c], Saket Asthana[a,]

a Advanced Functional Materials Laboratory, Department of Physics, ODF Campus, Yeddumailaram, Indian Institute of Technology Hyderabad, Andhra Pradesh-502205, India
b Department of Materials Science and Engineering, Indian Institute of Technology Hyderabad, Andhra Pradesh-502205, India
c Advanced Magnetics Group, Defence Metallurgical Research Laboratory, Kanchanbagh, Andhra Pradesh-500058, India

Solid State Communications
Volume 152, Issue 23, December 2012, Pages 2071–2077

http://dx.doi.org/10.1016/j.ssc.2012.08.007

Study of Structural, Magnetic and Electrical properties on Ho – substituted $BiFeO_3$

T. Durga Rao[a], T. Karthik[a,b], Adiraj Srinivas[c], Saket Asthana[a] *

[a] *Advanced Functional Materials Laboratory, Department of Physics,*

Indian Institute of Technology Hyderabad, Andhra Pradesh – 502205, India

[b] *Department of Materials Science and Engineering, Indian Institute of Technology Hyderabad, Andhra Pradesh – 502205, India*

[c] *Advanced Magnetics Group, Defense Metallurgical Research Laboratory, Kanchanbagh,*

Andhra Pradesh -500058, India

***** Author for Correspondence: asthanas@iith.ac.in

ABSTRACT

The polycrystalline $Bi_{1-x}Ho_xFeO_3$ (x = 0, 0.05, 0.1) compounds were synthesized by conventional solid-state route. Rietveld refinement revealed that all the compounds were stabilized in rhombohedral structure with *R3c* (IUCr No. 161) space group. Room temperature magnetic measurements revealed that Ho substitution induces ferromagnetism and improves the magnetic properties of $BiFeO_3$. A competing ferro and anti-ferro magnetic interaction was observed in these compounds. Temperature variation of complex impedance studies revealed that electrical properties are improved with the Ho substitution. The ac conductivity found to obey universal power law and showed the negative temperature coefficient of resistance character. Correlated Barrier Hopping model (CBH) was employed to explain the frequency and temperature dependence of ac conductivity and the mechanism of transport in the material BFO and Ho substituted BFO. Density of states near Fermi level was calculated by using the ac conductivity data.

Key words: A. Multiferroics, D. Electrical impedance, D. A.C conductivity, D. Correlated Barrier Hopping.

1. Introduction

Materials which exhibit simultaneous presence of magnetic and electric ordering are called multiferroics [1-3]. These materials have been studied due to their potential applications for electronic devices and interesting physics involved. $BiFeO_3$ (BFO) is a well-known multiferroic at room temperature having para- to ferro-electric transition temperature $T_C \sim 1103K$ and a G-type antiferromagnetic transition at $T_N \sim 643K$ [4]. BFO, in its bulk form, crystallizes in rhombohedral structure with R3c space group. In BFO, ferroelectricity arises due to the

stereochemical activity of $6s^2$ lone pair electrons of Bi^{3+}, while the indirect magnetic exchange interaction between Fe^{3+} ions through O^{2-} causes G-type antiferromagnetic ordering. But, BFO has a serious drawback of high leakage current due to either the presence of impurities or oxygen vacancies which promotes the low resistive path for conduction. To reduce the leakage current and to understand the underlying mechanism, various methods have been employed [5, 6]. To improve the physical properties, substitution is one of the best techniques [7-9]. Generally, rare earth ions or divalent alkaline earth ions will be substituted at A- (here Bi) site and transition metal elements at B- site (here Fe). But substitution of divalent ions at A- site may increase the oxygen vacancies [10] in order to make charge neutrality in the compound. This will enhance the leakage current which will deteriorate the electric properties of the compounds. So the multiferroic nature of the compounds can be improved by substitution of rare earth elements at A- site which creates internal chemical pressure within the lattice. This internal chemical pressure plays an important role to suppress the leakage current and improve the electric and magnetic properties [11]**.** It has been reported that substitution of lanthanides like La^{3+} [12]**,** Nd^{3+} [13]**,** Eu^{3+} [14] and Gd^{3+} [15] for Bi^{3+} in BFO would affect the crystal structure which in turn show an improved magnetic and electric properties. There are some reports on dielectric properties and impedance spectroscopy studies on BFO [16-18]. But to the best of our knowledge, there is no detailed study on ac conductivity and charge carrier mechanism in BFO. In this report, we have studied the electrical properties of BFO and substituted BFO. We have employed correlated barrier hopping model to describe the charge carrier mechanism and calculating the number of density of states near Fermi surface for the first time to our knowledge for BFO.

In this present work, Ho^{3+} ion has been chosen to substitute for Bi^{3+} ion due to its smaller ionic radius (1.015 Å) as compared to Bi^{3+} (1.17 Å). The Ho^{3+} ions will create internal chemical

pressure which will effect significantly the distortion in the structure. This distortion presumably may improve the physical properties of the system.

2. Experimental Details

BFO and $Bi_{1-x}Ho_xFeO_3$ (BHFO) [x = 0.05 (BHFO5), 0.1 (BHFO10)] polycrystalline compounds were synthesized by conventional solid-state reaction technique using the high purity Bi_2O_3, Fe_2O_3 and Ho_2O_3 (purity > 99.9%) as starting materials. These powders were mixed with their stoichiometric ratios and ground thoroughly for 2h. The powders were calcined in two step process at 780°C for 2h and then at 815°C for 3h. The calcined powder were pelletized in the form of circular disc of size 8 mm diameter and 1.5 mm thickness and sintered at 815°C for 3h with a heating rate of 5°C / min. The Phase analysis of the compounds were examined by an X-ray diffractometer (Panalytical X'pert Pro) with Cu K_α radiation (λ=1.5406 Å) with a 2θ step size of 0.016° over the angular range $20° \leq 2\theta \leq 70°$. Raman scattering spectra were measured at room temperature using a Laser Micro Raman spectrometer (Bruker, Senterra) with an excitation source of 785nm. The laser power of 10mW was used, so that sample heating was insignificant. The data were collected with each increment of $0.5cm^{-1}$ and an integration time of 10s. The magnetic properties of these compounds were measured using vibration sample magnetometer (ADE systems, Model no-EV9, USA). Deferential scanning calorimetry (DSC) was performed on a TA-Q200 calorimeter at a heating rate of 10°C / min under N_2 atmosphere, which has an accuracy of +/– 0.1°C. Dielectric properties were measured on the silver electrode compounds using Wayne Kerr 6500B impedance analyzer up to a frequency of 1MHz.

3. Results and discussion

3.1. Structural Properties

Fig. 1 shows the XRD patterns of polycrystalline BFO and BHFO compounds. Inserts 1(a) and 1(b) show the enlarged view of the XRD patterns from 27° - 31° and 31° - 33°. All the compounds crystallize in rhombohedral structure and their corresponding Bragg reflections were indexed with *R3c* space group. A trace amount of secondary phases like $Bi_2Fe_4O_9$ and $Bi_{25}FeO_{40}$ is observed along with the main phase (BFO) [19, 20]. But with the substitution of Ho, the intensity of secondary phases decreases from ~5% (BFO) to ~2% (BHFO) as estimated from XRD intensity profile. It is worth to mention that an evidence for structural phase separation has been observed in BHFO10 compound due to coexistence of nominal presence of orthorhombic phase along with parent *R3c* phase as shown in insert (a) of Fig. 1. A similar kind of observations for structural phase separation was reported in RE-substituted BFO ceramics [21, 22]. Lattice parameters are refined with *R3c* space group in a hexagonal unit cell using Full Prof software. The variation in structural parameters can be understood by Goldschmidt tolerance factor t, defined as $t = (\langle r_A \rangle + r_O)/\sqrt{2}(r_B + r_O)$ where $\langle r_A \rangle$ is the average radius of Bi^{3+} and Ho^{3+} ions at A site and r_B and r_o are the radii of Fe^{3+} and O^{2-} respectively. As the Ho content increases, the average A-site ionic radius decreases, which consequently lead to a decrease in tolerance factor values. This means that crystal structure will change from high symmetric state to low symmetric state. Due to this crystal distortion, lattice parameters, bond angles and bond distances will change. A systematic variation in the lattice parameters and Fe-O-Fe bond angles have been observed with the increase of Ho content which in turn consistent with an average A–site ionic radii ($\langle r_A \rangle$). The volume of the unit cell decreases continuously with the Ho content, which is due to the smaller ionic radius of Ho^{3+} as compared to that of Bi^{3+}. Variation of lattice parameters, bond angles and bond distances of BFO and BHFO compounds are given in the table 1. Further refinement studies are required to understand the phase separation in BFHO10.

3.2. Raman scattering spectra

Fig. 2 shows the Raman spectra of BFO and BHFO polycrystalline compounds. The measured spectra was fitted and decomposed into individual Lorentzian components to obtain the peak position of the each component i.e., natural frequency (cm^{-1}) of each Raman mode. For Rhombohedral (*R3c*) $BiFeO_3$, the Raman active modes can be summarized using the following irreducible representation: $\Gamma = 4A_1+9E$ [23-25]. Table 2 shows the Raman modes of BFO and BHFO compounds. The observed modes are in close agreement with that of Fukumura et al [25]. The low frequency peaks at 140.1, 172.4 and 228.2 cm^{-1} can be assigned as A_1-1, A_1-2 and A_1-3 respectively. The remaining eight peaks at 130.4, 261.0, 274.4, 346.3, 369.9, 412.8, 469.7 and 526.4 cm^{-1} can be assigned as E modes. An additional Raman mode (shown by an arrow) at 291.5cm^{-1} may correspond to the phonon mode of secondary phase $Bi_2Fe_4O_9$ [26, 27]. This particular phonon mode smears out with Ho substitution due to suppression of secondary phases which is also consistent with XRD results. With the increase of Ho, the strength of Bi-O covalent bonds will be changed due to the decline of stereochemical activity of Bi lone pair electrons. The modes A_1-1, A_1-2, A_1–3 and E-2 are governed by Bi-O covalent bonds. As the Ho content increases in BFO, the frequency of these modes shift gradually to higher frequency side. If *k* is the force constant and ***M*** is the reduced mass, then the frequency of the mode is proportional to $(k / \boldsymbol{M})^{½}$ provided it is governed by the local factors [28]. If we assume the radius of Ho^{3+} ion is same as the radius of Bi^{3+}, since the valence of Ho^{3+} is same as that of Bi^{3+}, *k* is assumed to be independent of substitution as a zero approximation. As the mass of Ho^{3+} ion is 21% less than the mass of Bi^{3+} ion, the relatively light Ho^{3+} ion may increase the frequency of vibration of the modes.

3.3. Magnetic properties

Isothermal magnetization (*M – H*) curves of BFO and BHFO compounds have been recorded up to a maximum magnetic field of 20 kÖe at room temperature as shown in Fig. 3. In

BFO, the Fe^{3+} magnetic moments are coupled ferromagnetically in the pseudo cubic (111) planes, but antiferromagnetically between the adjacent planes. The existence of superimposition of spiral modulated spin structure with the G-type antiferromagnetic spin ordering prevents both the observation of any net magnetization and the linear magnetoelectric effect. The existence of a weak ferromagnetic moment is permitted by the crystal symmetry of BFO [29]. As the Ho content increases, the average radius at Bi-site decreases. This will create the change in the interatomic distances and the Fe – O – Fe bond angle deviation from 180^o [30]. This bond angle controls the superexchange interaction between the antiferromagnetically aligned Fe^{3+} ions through the intervening oxygen anions. The Fe – O – Fe bond angle changes with Ho- content which inturn felicitates the dominance of ferromagnetic interactions over antiferromagnetic interactions. Therefore, weak ferromagnetism in these compounds presumably due to the internal chemical pressure induced by Ho- substitution, which leads to suppression of the spatially modulated spiral spin structure and hence the net magnetization in it [31]. Insert (a) in Fig. 3 shows the enlarged view of magnetization data near origin. The remanent magnetizations M_r of BFO, BHFO5, BHFO10 compounds, are respectively 0.0013, 0.0064 and 0.0943 emu/g. The remanent magnetization M_r of BHFO10 compound is nearly increased by one order of magnitude as compared to BFO. A non linear variation of magnetization with the applied magnetic field is observed for BHFO10 compound. There are three nearly closed loops in the M – H curve for this compound. One is very narrow loop symmetrically situated between ±0.5 kOe arising from ferromagnetic interactions, and two loops lying between ±0.5kOe and ±20 kOe arising from antiferromagnetic interactions. The area enclosed by the first loop is insignificant compared to the other loops. But when the magnetization is measured at temperature 20K (not shown here) for this compound, the loop between ±0.5 kOe becomes broader where as the other two loops become narrow. Similar kind of behavior was observed by one of the authors in

manganites [8] and by M. A. Manekar et al in $Ce(Fe_{0.96}Al_{0.04})_2$ [32]. This behavior is giving a sign of competitions between ferromagnetic and antiferromagnetic interactions. With the decrease of temperature, ferromagnetic interactions increase at the expense of antiferromagnetic interaction.

From the Differential scanning calorimetry (DSC), the antiferromagnetic to paramagnetic transition temperature T_N was observed as shown in insert (b) of Fig. 3. Insignificant variation (from 373°C for BFO to 375°C for BHFO10) in T_N was observed which is in agreement with reported findings for A site substituted BFO [33, 34]. Although, T_N variation is insensitive to Ho-content, however, increasing trend can be accounted due to variation in Fe-O-Fe bond angle as revealed from our XRD refinement data. The variation of T_N with Fe-O-Fe bond angle can be explained the following equation [35]

$$T_N = JZS(S+1)\cos\theta \quad (1)$$

Where J the exchange is constant, S is the spin of Fe^{3+}; Z is the average number of linkages per Fe^{+3} ions and θ is Fe – O – Fe bond angle. As the Ho content increases, the bond distances and bond angles will change due to the decrease of tolerance factor. The enhancement of T_N is due to the reduction of Fe – O distance and increase of Fe – O – Fe bond angle. Since in the above equation, T_N is proportional to the cosine of the bond angle which increases with the increase of bond angle and consistence with our observations.

3.4. Impedance studies

Fig. 4 shows the frequency dependence of real and imaginary parts of impedance (Z′ and Z″) for BFO and BHFO at 30°C. The value of Z′ decreases drastically until 1 kHz and

approaches a constant value up to 1MHz. Decrease in Z' with frequency indicates the presence of dielectric relaxation behavior in these compounds [36].

Z' and Z'' decrease monotonically below 150°C to room temperature with the increase of frequency and attain a constant value at high frequency region (similar to room temperature behavior as shown in Fig. 4). The value of Z' shows the same trend even in the temperature range from 30°C to 190°C as shown in Fig. 5 (a-c) which is unlike in the Z'' variation (discussed in next paragraph). The existence of negative temperature coefficient of resistance (NTCR) in these compounds can be accounted in terms of decrement in Z' with temperature at low frequency region. The overlapping of Z' plots at high frequency region may be due to the release of space charge polarization and reduces the barrier properties in these materials [37]. An enhancement of the bulk resistance of the compounds can be accounted due to the decrease of conduction path with Ho-content [38].

Fig. 5 (d-f) shows frequency dependence of the imaginary part of impedance (Z'') of BFO and BHFO compounds from 150°C to 190°C. The electrical relaxations are significantly absent within the investigated frequency range below 150°C (not shown here) [39]. Above 150°C, Z'' data is characterized by i) appearance of a peak with a maximum value (Z''_{max}) at a certain frequency, ii) asymmetrical broadening, iii) shifting of Z''_{max} value to higher frequency with temperature and iv) decrement in magnitude of Z''_{max} with the temperature. Appearance of peak indicates the presence of electrical relaxation in all the compounds. Asymmetric broadening suggests that there is a distribution of spread of relaxation times. A signature of concentration dependent relaxation process is observed in terms of decrement in width of asymmetric broad peak. Further, shifting of Z''_{max} value to the higher frequency side with temperature indicates the existence of temperature dependent electrical relaxation phenomenon in the material [38, 40]. At a given temperature (say 150°C-190°C), the magnitude of Z''_{max} increases and the peak in Z''

shifts to the low frequency side with the Ho content in BFO. This observation may be attributed due to a phenomenon with maximum capacitive effects due to Ho substitution [36].

3.5 AC Conductivity studies

Fig. 6 shows the frequency variation of ac conductivity at different temperatures. The response of the material to the applied electric field is described by the ac conductivity. The nature of transport process will be known by ac conductivity studies. The ac electrical conductivity was calculated by using the relation,

$$\sigma_{ac} = l/SZ' \quad (2)$$

where l is the thickness and S is the surface area of the pellet.

At room temperature, the frequency dependence of ac conductivity obeys the universal power law [41]

$$\sigma_{ac} = A\omega^{s} \quad (3)$$

Above room temperature this dependence follows the equation [42]

$$\sigma_{ac} = A_1\omega^{s}{}_1 + A_2\omega^{s}{}_2 \quad (4)$$

where A, A_1 and A_2 are temperature dependent parameters and s, s_1 and s_2 are both temperature and frequency dependent parameters. The values of s_1 and s_2 are determined by the slopes in the low and high frequency regions respectively. But from the observed data, s values are lower than 1 and decrease with the increase of temperature. With the increase of temperature, the value of s_1 is decreasing and approaching to zero at high temperature. This indicates that at high temperatures and at low frequencies, the dc conductivity dominates and obeys Joncher's power law [43]:

$$\sigma_{ac} = \sigma(0) + A\omega^{s}$$
$$= \sigma(0) + \sigma(\omega) \quad (5)$$

where σ (0) is the frequency independent part of conductivity.

At low frequencies, as the temperature increases, σ_{ac} is very nearly equal to σ (0) due to inter-well hopping which is responsible for dc conduction. As the frequency increases, ac conductivity σ (ω) increases which is presumably due to dominance of intra-well hopping over the inter-well hopping.

Generally, in the case of Quantum Mechanical Tunneling (QMT) through the barrier separating the two localized sites, s should be independent of temperature and slightly decreases with frequency while in the case of Correlated Barrier Hopping (CBH), s should decrease with the increase of temperature. Fig. 6 shows the temperature dependence of ac conductivity. Inserts in Fig. 6 show the temperature dependence of s. It is observed from the figure that s values are less than 1 and decreasing with temperature. Further the values of s in the low frequency region decreases and approaches to zero as the temperature is increased. So the observed data is consistent with the CBH model. This indicates that the conduction process is thermally activated. These materials have their band gaps similar to that of semiconductor and hopping conduction mechanism in these materials is generally consistent with the existence of a high density of states. Polarons are formed due to localization of charge carriers and the hopping conduction may occur between the nearest neighboring sites [44].

Based on the CBH model, the number of density of states $N(E_f)$ near the Fermi level was calculated by the ac conductivity data by using the following relation [45]

$$\sigma_{ac} = \frac{\pi}{3} e^2 \omega k_B T \left[N\left(E_f\right)\right]^2 \alpha^{-5} \left(ln\frac{f_o}{\omega}\right)^4 \quad (6)$$

Where f_o is the photon frequency and α is the localized wave function, assuming $f_o = 10^{13}$ Hz and the polarizability $\alpha = 10^{10}$ m^{-1} at various operating temperatures and frequencies. Fig. 7(a-c) shows frequency dependence of number of states $N(E_f)$ for BFO and BHFO compounds at

different temperatures. It is observed from the figures that the number of states $N(E_f)$ decreases with the operating frequency for BFO and BHFO5 at all temperatures, whereas for BHFO10, the same increases with the frequency up to 100°C. Above 100°C, $N(E_f)$ decreases showing a minimum and then increases. The minimum in $N(E_f)$ shifts to higher frequency side with the increase of temperature. At a constant temperature, the decrease of number of states with the increase of Ho content in BFO may be due to the reduction of oxygen vacancies in these compounds. The number of states $N(E_f)$ increases with the increase of temperature at a given frequency. The reasonably high density of states $N(E_f)$ indicates that hopping between the pairs of sites dominates the mechanism of charge transport in these compounds.

Conclusions

Polycrystalline $Bi_{1-x}Ho_xFeO_3$ (x = 0, 0.05, 0.1) compounds were synthesized by conventional solid state route. All the compounds crystallize in the class of rhombohedral structure with R3c space group. A systematic structural distortion has been observed with Ho-substitution in BFO as evident from XRD and Raman spectrum analysis. With the increase of Ho content in BFO, ferromagnetic interactions dominate at the expense of antiferromagnetic interactions which are also supported by low temperature M-H data. It is worth to mention that occurrence of two M-H loops of different origin is a signature of magnetic phase separation which is due to the simultaneous presence of ferro-and antiferromagnetic phases. Insignificant variation in T_N has been observed and explained with Fe-O-Fe bond angle in Ho-substituted BFO. The bulk resistance of the compounds was enhanced with the Ho content. The ac conductivity found is to obey universal power law and showed the negative temperature coefficient of resistance character. The frequency variation of ac conductivity at different temperatures indicates that the conduction process is thermally activated. These results are well supported by density of states near Fermi level.

References:

[1] W. Prellier, M.P. Singh, and P. Murugavel, J. Phys.:Condens. Matter. 17 (2005) R803.

[2] W. Eerenstein, N.D. Mathur, J.F. Scott, Nature 442 (2006) 759.

[3] G. Catalan, J.F. Scott, Adv. Mater. 21 (2009) 1.

[4] J.B. Neaton, C. Ederer, U.V. Waghmare, N.A. Spaldin, K.M. Rabe, Phys. Rev. B 71 (2005) 014113.

[5] Xiaoding Qi, Joonghoe Dho, Rumen Tomov, G. Mark. Blamire, L. Judith, MacManus-Driscoll, Appl. Phys. Lett. 86 (2005) 062903.

[6] Mikael A. Khan, Tim P. Comyn, Andrew J. Bell, Appl. Phys. Lett. 92 (2008) 072908.

[7] Nari Jeon, Dibyaranjan Rout, Ill Won Kim, and Suk-Joong L. Kang, Appl. Phys. Lett. 98 (2011) 072901.

[8] C.M. Srivastava, R.K. Dwivedi, Saket Asthana, A.K. Nigam, D. Bahadur, J. Magn. Magn. Mater. 284 (2004) 239.

[9] G. L. Yuan, Siu Wing Or, J. M. Liu, Z. G. Liu, Appl. Phys. Lett. 89 (2006) 052905.

[10] V A Khomchenko, M. Kopcewicz, A. M. L. Lopes, Y. G. Pogorelov, J. P. Araujo, J. M. Vieira, A.L. Kholkin, J. Phys. D: Appl. Phys. 41 (2008) 102003.

[11] S.T. Zhang, Y. Zhang, M.H. Lu, C.L. Du, Y.F. Chen, Z.G. Liu, Y.Y. Zhu, N.B. Ming, X.Q. Pan, Appl. Phys. Lett. 88 (2006) 162901.

[12] Z. X. Cheng, X.L. Wang, S.X. Dou, Phys. Rev. B. 77 (2008) 092101.

[13] H. Uchida, R. Ueno, H. Funakubo, S. Koda, J. Appl. Phys. 100 (2006) 014106.

[14] A. Lahmar, S. Habouti, M. Dietze, C.H. Solterbeck, M. Es-Souni, Appl. Phys. Lett. 94 (2009) 012903.

[15] Renqing Guo, Liang Fang, Wen Dong, Fengang Zheng, and Mingrong Shen, J. Phys. Chem. C 114 (2010) 21390.

[16] Hemant Singh, Amit Kumar, K.L. Yadav, Mat. Sci. & Engg. B, 176 (2011) 540-547.

[17] Amar Srivastava, Ashish Garg, Finlay D. Morrison, J. Appl. Phys. 105 (2009) 054103.

[18] Jhih-Cyun Chen, Jenn-Ming Wu, Appl. Phys. Lett. 91 (2007) 182903.

[19] I. Sosnowska, T. Peterlin-Neumaier, E. Steichele, Phys C 15 (1982) 4835.

[20] C. Tabares-Munoz, J. P. Rivera, A. Monnier, H. Schmid, Jpn. J. Appl. Phys. 24 (1985) 1051.

[21] V.A. Khomchenko, V.V. Shvartsman, P. Borisov, W. Kleemann, D.A. Kiselev, I.K. Bdikin, J.M. Vieira, A.L. Kholkin, Acta Mater. 57 (2009) 5137-5145.

[22] Xingquan Zhang, Yu Sui, Xianjie Wang, Yang Wang, Zhu Wang, J. Alloys Compd. 507 (2010) 157-161.

[23] Manoj K. Singh, Hyun M. Jang, Sangwoo Ryu, Moon-Ho Jo, Appl. Phys. Lett. 88 (2006) 042907.

[24] R. Haumont, J. Kreisel, P. Bouvier, F. Hippert, Phys. Rev. B 73 (2006) 132101.

[25] H. Fukumura, H. Harima, K. Kisoda, M. Tamada, Y. Noguchi, M. Miyayama, J. Magn. Magn. Mater. 310 (2007) 367.

[26] Alexandra Friedrich, Jasmin Biehler, Wolfgang Morgenroth, Leonore Wiehl, Bjorn Winkler, Michael Hanfland, Martin Tolkiehn, Manfred Burianek, Manfred Muhlberg J. Phys.: Condens. Matter 24 (2012) 145401.

[27] M.N. Iliev, A.P. Litvinchuk, and V.G. Hadjiev, M.M. Gospodinov, V. Skumryev, E. Ressouche, Phys. Rev. B 81 (2010) 024302.

[28] D. Wu, Y. Deng, C.L. Mak, K.H. Wong, A.D. Li, M.S. Zhang, N.B. Ming, Appl. Phys. A 80 (2005) 607.

[29] A.M. Kadomtseva, F.Y. Popov, A.P Pyatakov, G.P. Vorob'ev, A.K. Zvezdin, D. Viehland, Phase Transitions, 79 (2006) 1019.

[30] M.B. Bellaki, V. Manivannan, C. Madhu, A. Sundaresan, Materials Chemistry and Physics, 116 (2009) 599.

[31] I. Sosnowska, W. Schaefer, W. Kockelmann, K.H. Andersen, I.O Troyanchuk, Appl. Phys. A **74** (2002) 1040.

[32] M.A. Manekar, S. Chaudhary, M.K. Chattopadhyay, K. J. Singh, S.B. Roy, P. Chaddah, Phys. Rev. B 64 (2001) 104416.

[33] Deepti Kothari, V. Raghavendra Reddy, Ajay Gupta, Vasant Sathe, and A. Banerjee, S. M. Gupta, A.M. Awasthi, Appl. Phys. Lett. 91 (2007) 202505.

[34] Stefan Saxin, Christopher S. Knee, J. solid state chem, 184 (2011) 1576-1579.

[35] M.A. Ahmed, S.I El-Dek, Mat. Lett. 60 (2006) 1437.

[36] Amar Srivastava, Ashish Garg, Finlay D. Morrison, J. Appl. Phys. 105 (2009) 054103.

[37] A. Kumar, B.P. Singh, R.N.P. Choudhary, A.K. Thakur, Mater. Chem. Phys. 99 (2006) 150.

[38] Hemant Singh, Amit Kumar, K.L. Yadav, Mat Sci Eng B 176 (2011) 540–547.

[39] S. Sen, S.K. Mishra, S.K. Das, A. Tarafdar, J. Alloys Compd. 453 (2008) 395.

[40] C.K. Suman, K. Prasad, R.N.P. Choudhary, Adv. Appl. Ceram. 104 (2005) 294.

[41] N.F. Mott, E.A. Davis, Electronic Processes in Non-Crystalline Materials, Oxford University Press, London (1979).
[42] K. Funke, Prog. Solid State Chem. 22 (1993) 111.
[43] A.K. Jonscher, Nature 267 (1977) 673.
[44] K. Prasad, Chandra, K.P. Priyanka, A.R. Kulkarni, J. Mater. Sci. 46 (2011) 2077.
[45] G.D. Sharma, M. Roy, M.S. Roy, Mater. Sci. Eng. B 104 (2003) 15.

Figure captions

Fig. 1. X- ray diffraction patterns of BFO and BHFO compounds. ***, #** indicate peaks due to $Bi_2Fe_4O_9$ and $Bi_{25}FeO_{40}$ respectively. Inserts (a) and (b) show the enlarged view of the XRD patterns from 27 - 31° and 31 - 33°.

Fig. 2. Raman scattering spectra of BFO and BHFO compounds at room temperature.

Fig. 3. Isothermal magnetization curves at room temperature for BFO and BHFO compounds. Insert 3(a) and 3(b) show M-H plot with enlarged view near the origin and DSC plots of the compounds respectively.

Fig. 4. Frequency dependence of real part of impedance Z′ for BFO and BHFO compounds. Insert shows frequency dependence of Z″ for BFO and BHFO compounds.

Fig. 5. (a) - (c) Frequency dependence of real part of impedance (Z′) and (d) - (f) Frequency dependence of imaginary part of impedance (Z″).

Fig. 6. Frequency dependence of a.c conductivity of BFO (a), BHFO5- (b) and BHFO10- (c) compounds.

Fig. 7. Variation of density of states at Fermi level of BFO (a), BHFO5- (b) and BHFO10- (c) compounds with frequency at different temperatures.

Figures:

Figure – 1

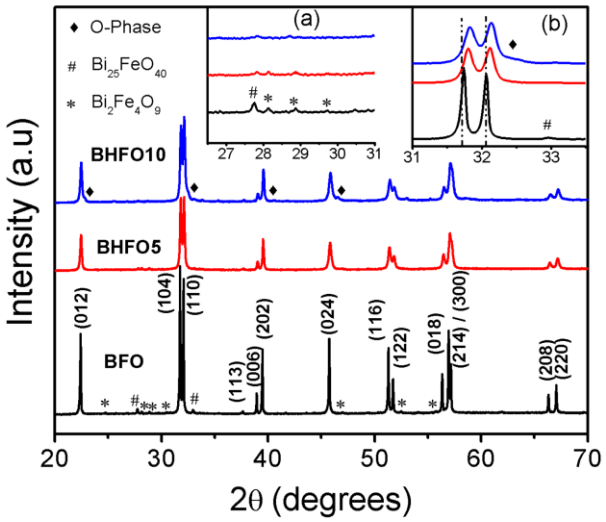

Figure – 2

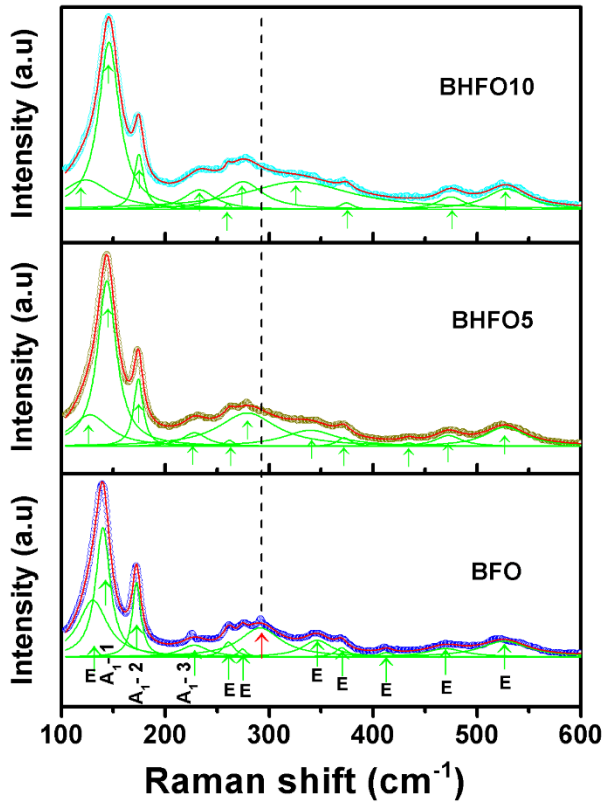

Figure – 3

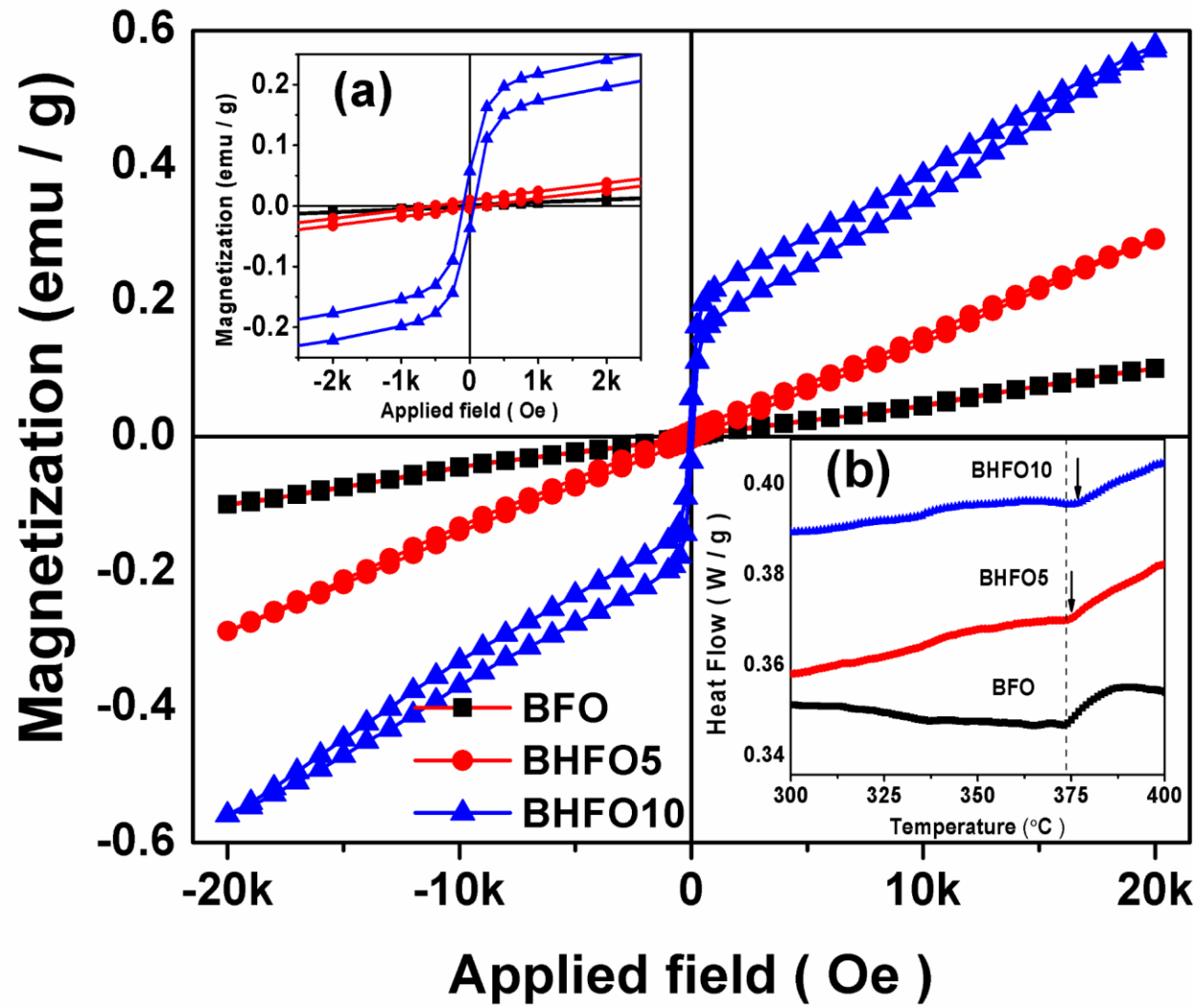
Magnetization (emu / g)
Applied field (Oe)
0.6
0.4
0.2
0.0
-0.2
-0.4
-0.6
-20k
-10k
0
10k
20k
BFO
BHFO5
BHFO10
(a)
Magnetization (emu / g)
0.2
0.1
0.0
-0.1
-0.2
-2k
-1k
0
1k
2k
Applied field (Oe)
(b)
BHFO10
BHFO5
BFO
Heat Flow (W / g)
0.40
0.38
0.36
0.34
300
325
350
375
400
Temperature (°C)

Figure – 4

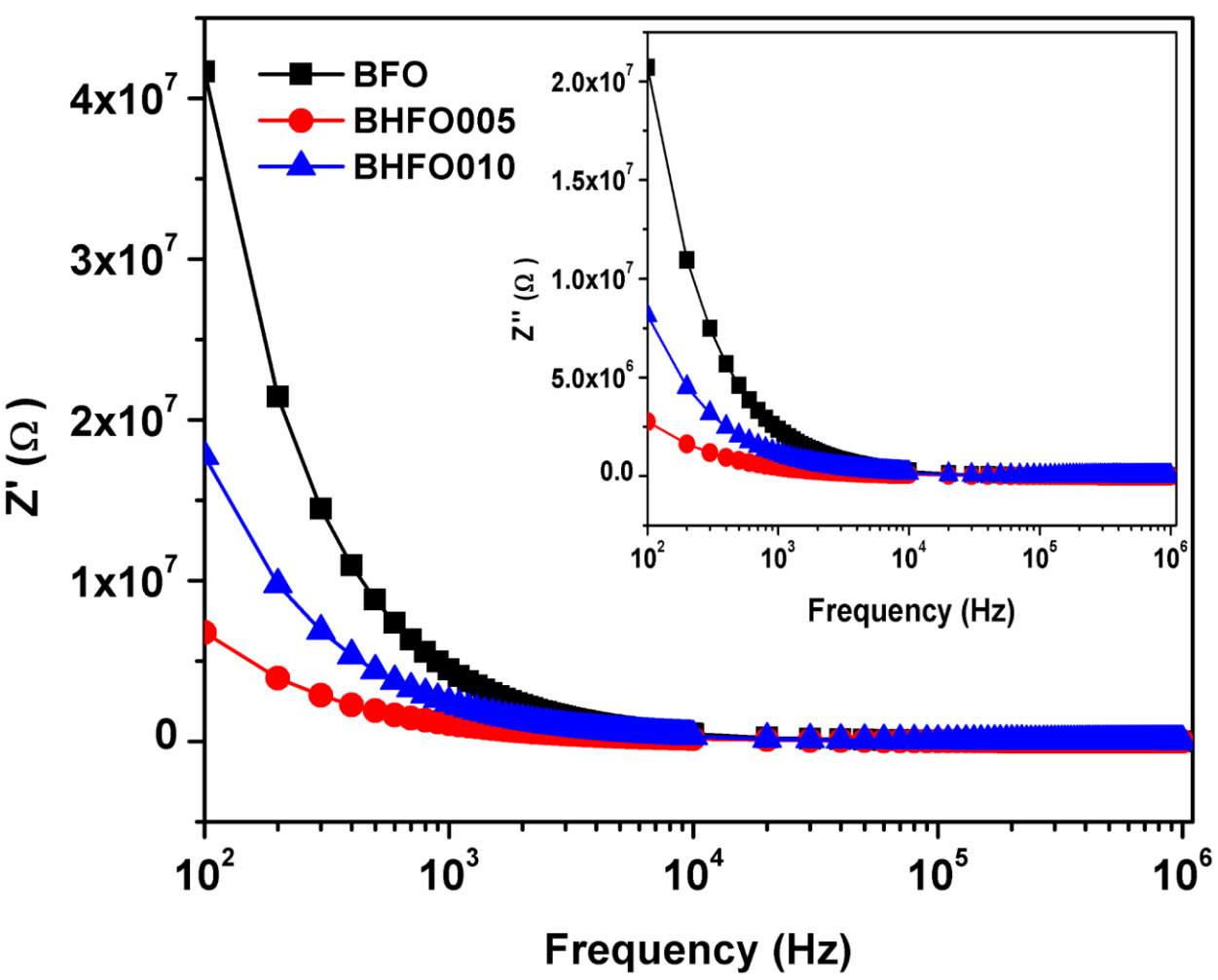
BFO
BHFO005
BHFO010
Z' (Ω)
4x10^7
3x10^7
2x10^7
1x10^7
0
10^2
10^3
10^4
10^5
10^6
Frequency (Hz)
Z'' (Ω)
2.0x10^7
1.5x10^7
1.0x10^7
5.0x10^6
0.0
10^2
10^3
10^4
10^5
10^6
Frequency (Hz)

Figure – 5

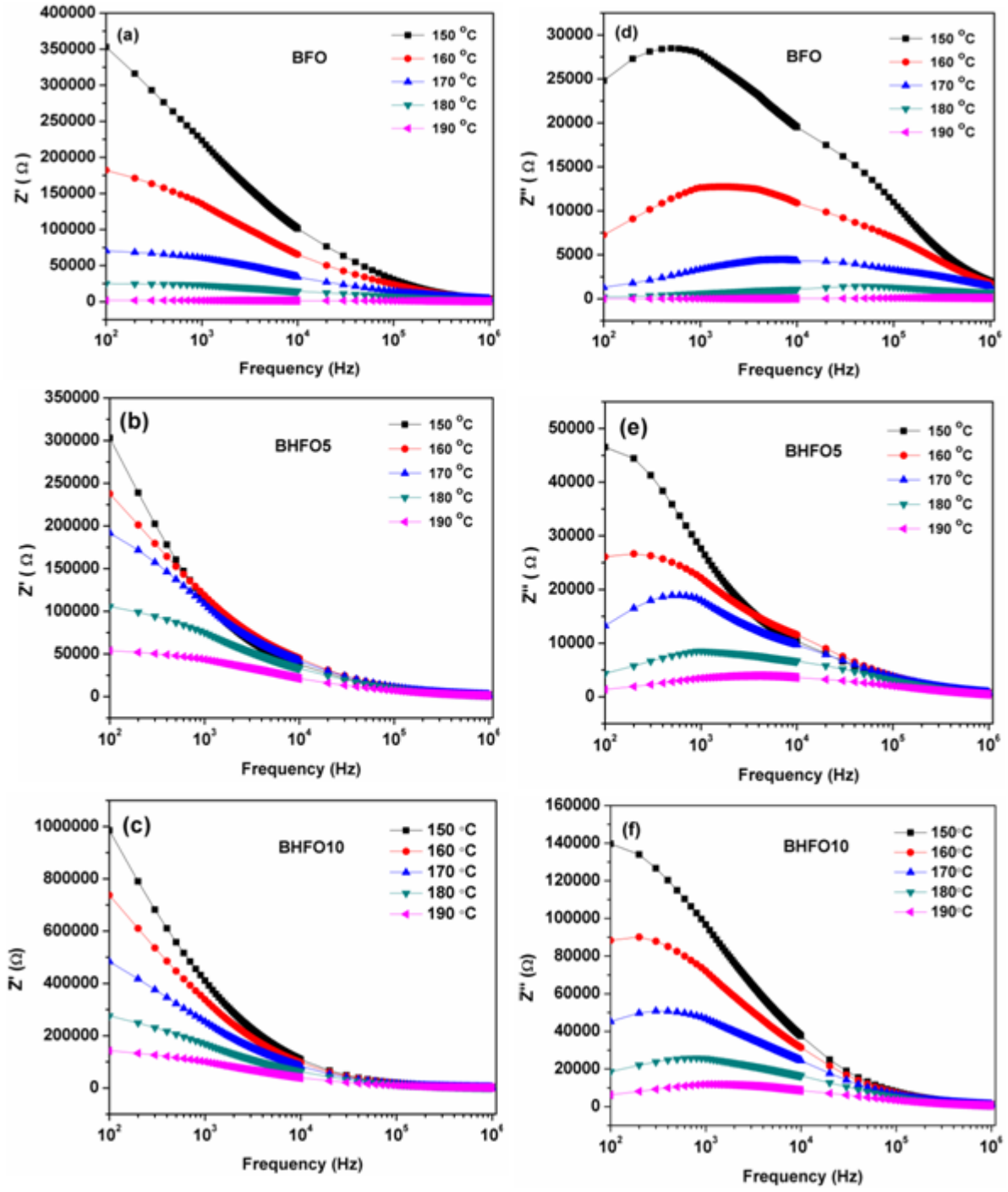
(a)
BFO
150 °C
160 °C
170 °C
180 °C
190 °C
Z' (Ω)
Frequency (Hz)
(d)
BFO
Z'' (Ω)
(b)
BHFO5
(e)
BHFO5
(c)
BHFO10
Z' (Ω)
(f)
BHFO10
Z'' (Ω)

Figure – 6

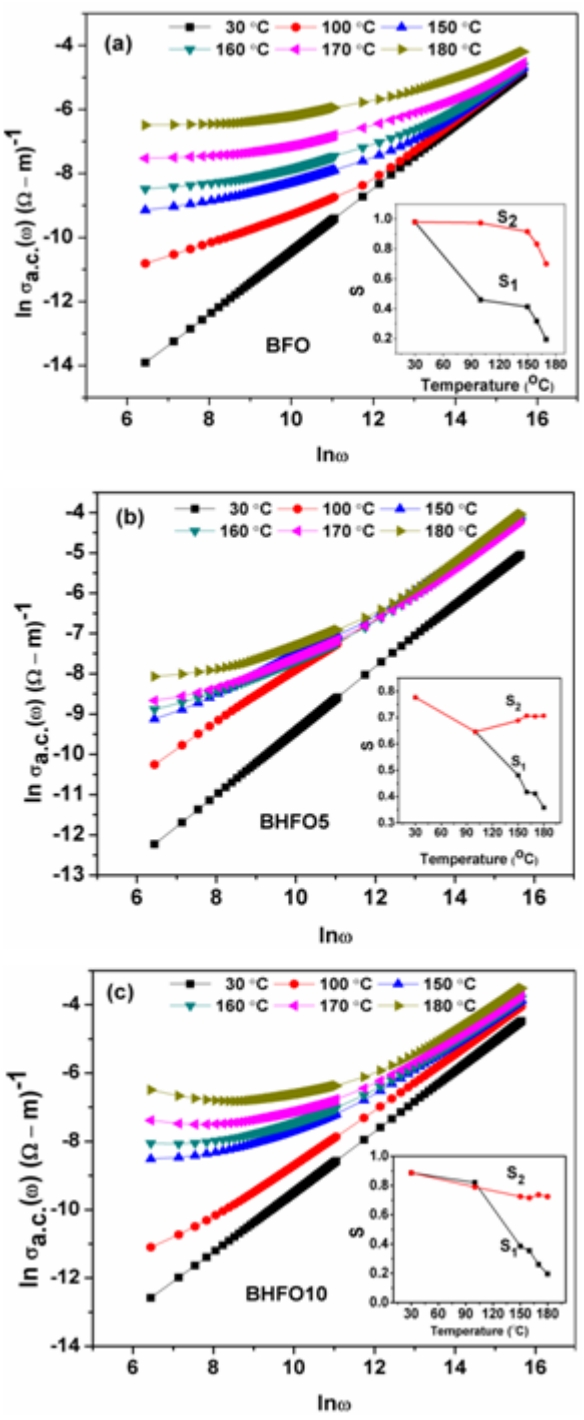
(a)
30 °C
100 °C
150 °C
160 °C
170 °C
180 °C
BFO
S2
S1
S
Temperature (°C)
ln σa.c.(ω) (Ω – m)-1
lnω
(b)
BHFO5
(c)
BHFO10

Figure – 7

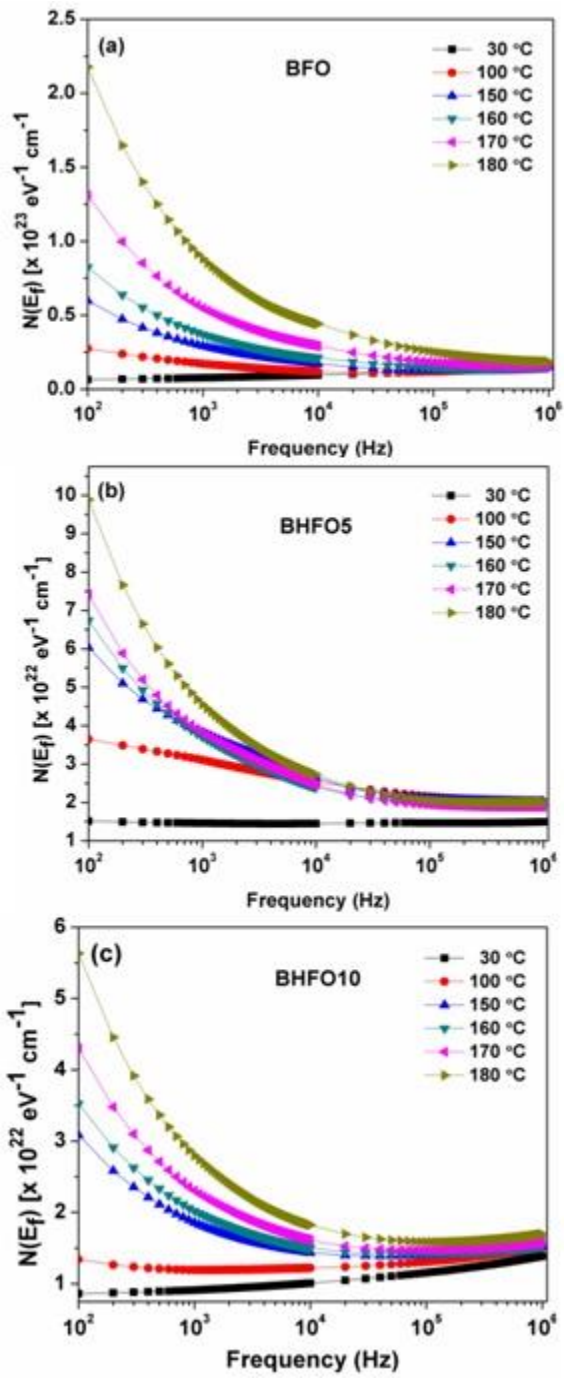
(a)
BFO
30 °C
100 °C
150 °C
160 °C
170 °C
180 °C
N(Ef) [x 10^23 eV^-1 cm^-1
Frequency (Hz)
(b)
BHFO5
N(Ef) [x 10^22 eV^-1 cm^-1]
Frequency (Hz)
(c)
BHFO10
N(Ef) [x 10^22 eV^-1 cm^-1]
Frequency (Hz)

Tables:

TABLE CAPTIONS:

Composition	a_{hex} (Å)	c_{hex} (Å)	V (Å)^3	Fe-O-Fe	Fe-O	τ
x = 0	5.5792(7)	13.8672(9)	373.83(3)	153.0(3)	1.98(6)	0.8886
x = 0.05	5.5740(1)	13.8494(7)	372.64(8)	156.2(3)	1.90(7)	0.8859
x = 0.10	5.5716(3)	13.8393(3)	372.05(7)	158.2(5)	1.87(8)	0.8831

Table. 1 Variation of lattice parameters, volume of the unit cell, bond angle and bond distance and tolerance factor with the Ho concentration

Raman modes	BFO	BHFO5	BHFO10
A_1-1(cm^{-1})	140.1	143.9	145.8
A_1-2(cm^{-1})	172.4	174.2	174.7
A_1-3(cm^{-1})	228.2	228.7	233.0
A_1-4(cm^{-1})	-	-	-
E(cm^{-1})	261.0	261.9	260.4
E(cm^{-1})	274.4	279.2	275.0
E(cm^{-1})	346.3	339.7	327.4
E(cm^{-1})	369.9	372.3	374.6
E(cm^{-1})	412.8	434.6	-
E(cm^{-1})	469.7	472.7	474.9
E(cm^{-1})	526.4	527.4	528.6
E(cm^{-1})	-	-	-
E(cm^{-1})	130.4	127.9	123.8

Table. 2. Raman modes of BFO and BHFO compounds.